AD-A139 459 STRESS STATES OF UNDERGROUND CAVE UNDER DETONATION LOAD 1/1
(U) FOREIGN TECHNOLOGY DIV WRIGHT-PATTERSON AFB OH
Y SHENGTIAN ET AL. 02 MAR 84 FTD-ID(RS)T-0116-84

UNCLASSIFIED F/G 13/13 NL

END
DATE FILMED
4-84
DTIC

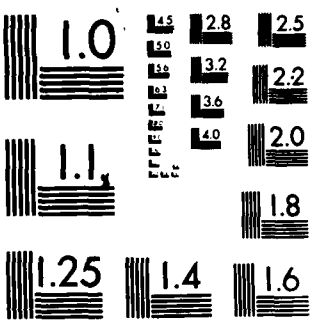

(2)

FTD-ID(RS)T-0116-84

AD A139459

FOREIGN TECHNOLOGY DIVISION

STRESS STATES OF UNDERGROUND CAVE UNDER DETONATION LOAD

by

Y. Shengtian and Z. Yaoqin

DTIC ELECTE S D MAR 2 8 1984 B

Approved for public release; distribution unlimited.

DTIC FILE COPY

84 03 27 074

EDITED TRANSLATION

FTD-ID(RS)T-0116-84 2 March 1984

MICROFICHE NR: FTD-84-C-000242

STRESS STATES OF UNDERGROUND CAVE UNDER DETONATION LOAD

By: Y. Shengtian and Z. Yaoqin

English pages: 15

Source: Dixia Gongcheng, Nr. 11, 1982, pp. 1-6

Country of origin: China
Translated by: LEO KANNER ASSOCIATES
F33657-81-D-0264
Requester: FTD/SDBF

PREPARED BY:

TRANSLATION DIVISION
FOREIGN TECHNOLOGY DIVISION
WP-AFB, OHIO.

GRAPHICS DISCLAIMER

All figures, graphics, tables, equations, etc. merged into this translation were extracted from the best quality copy available.

Accession For	
NTIS GRA&I	☑
DTIC TAB	☐
Unannounced	☐
Justification	
By	
Distribution/	
Availability Codes	
Dist	Avail and/or Special
A-1	

STRESS STATES OF UNDERGROUND CAVE UNDER DETONATION LOAD*

Yang Shengtian and Zhang Yaoqin

I. Computation Model

1. It is assumed that there is a cave in a mountain body (or underground), where the axial direction dimensions of the cave are considerably greater than the characteristic dimensions of the cave structure. Moreover, the axial direction dimensions are acted on by a cylindrical wave parallel to the longitudinal axis because of the strip-shaped detonation source. Hence, the strain simulation of the cave can be considered a problem of plane strain (Fig. 1).

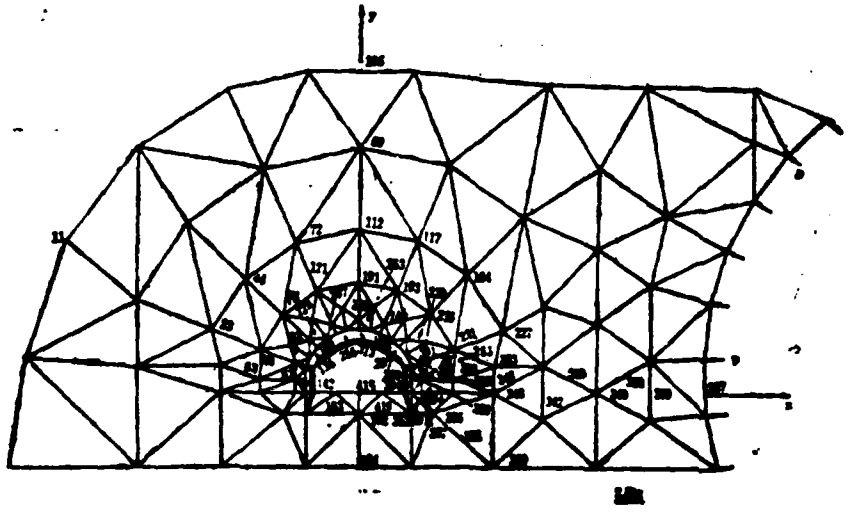

Fig. 1. Computation model.

* This article has been abridged by the journal.

2. The mountain body is composed of an isotropic homogeneous substance.

3. The model has three boundaries: the upper portion is the free boundary, satisfying the practical conditions of the mountain body; the mountain base is assumed to be the artificial boundary (the damping boundary). The remaining side (boundary) is due to loading.

4. The distance from the loading boundary (of the computation model) to the detonation center is about five times the span of the detonation chamber. In this article, the detonation center is used as the origin and the loading boundary is a circular-arc surface with center at the origin and radius of 30 meters. Thus, the inner portion can be considered as basically an elastic zone. The distance from the loading point to the center (the origin) of the cave is 32.5 meters.

5. The given boundary conditions of the load are radial loading under the cylindrical coordinates, and at any instant the load is at the normal direction of the wave train surface; these two magnitudes of load are the same. The detonation chamber and the cave are at the same elevation.

II. Load and Fundamental Parameter

1. The load waveform is assumed as triangular (Fig. 2).

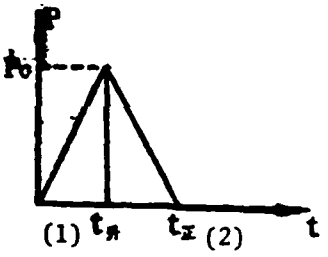

Fig. 2.
Key: (1) Ascending; (2) Positive.

$P=P_0(t/t_{\text{ascending}})$ when $t \geq t_{\text{ascending}}$.

$P=P_o[(t_{positive}-t)/(t_{positive}-t_{ascending})]$ when $t_{ascending}<t\leq t_{positive}$ and satisfying $t_{ascending}=(1/2)t_{positive}$.

2. The form of the cave is a straight-wall arch without lining, and the rise-span ratio is 0.31.

The medium parameters:

$E=1.4\times10^5$ kg/cm^2; $\rho=2.65$ tons/m^3;

$\nu=0.3$; $t_{positive}=0.002$ S;

$t_{ascending}=0.001$ S (or $=0$);

$\lambda=0.01$ (damping ratio); $L=9.7$ m (span);

$h=2.5$ m (wall height); $P_o=100$ kg/cm^2.

III. Computation Method

Beginning from the dynamic equilibrium equation of monolithic construction

$$[K]\{u\}-[c]\{\dot{u}\}+[M]\{u\}=\{k\}$$

a six-nodal-point triangular unit is utilized to solve (step by step) for the double-step-length method (the Wilson stable integration method when $\theta=2$). In the equation, [K], [c] and [M] are respectively the rigidity, damping and mass matrix, and {u}, {u̇}, and {ü} are respectively vectors of displacement, velocity and acceleration.

In the damping matrix $c=\alpha M+\beta K$, $\alpha=\lambda\omega_1$ and $\beta=\lambda/\omega_1$. ω_1 is the fundamental frequency of the model.

The mass matrix is used with the concentrated mass approximation method in physics.

As revealed by the computation, the magnitude of the damping ratio exerts a considerable influence on the dynamic reaction of the structure; moreover, the value of λ is related to the structure type, material property and load waveform. Assuming the damping ratio λ as 0.01, 0.02, 0.03, 0.05 and 0.08, from computation the stress waveforms of the nodal point at the boundary of the original load are considerably different from the given waveform; values of amplitude also obviously vary. Refer to Fig. 3 for changes of waveforms. Finally, it is assumed that $\lambda=0.01$ in the computation.

In addition:

1. Concerning the unit dimension

The sub-period of the selected unit is smaller than the period of the load waveform. Calculation of the sub-period uses the equation $T_z=H_e/C_p$. In the equation, H_e is the distance of a unit along the direction of wave propagation and C_p is wave velocity. According to the equation, in this article the unit $T_z=0.001$ second; the period of load waveform $T_o=0.004$ second (wave velocity C_p≈2500 m/sec at one unit dimension $H_e=2.5$ m). According to computation experience, the error in calculating stress cannot be too great (usually not exceeding 1.5 percent).

2. Duration of time segment dt

The selection of the duration of the time segment can affect the accuracy of numerical integration. As pointed out in Reference [1], when $dt/T<0.01$, the integration result is accurate; at that time, the period T can use the shorter value in the system and load. In this article, it is selected that $(dt/T)=0.025$. Usually, the error in the stress calculation does not exceed 2.5 percent.

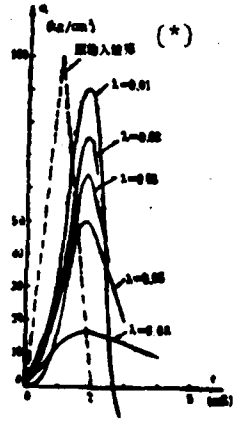

Fig. 3. Effects of damping ratio .
Key: (*) Original input waveform.

3. Boundary conditions

In order to have the boundary free from reflection of the wave (in other words the wave can smoothly pass through the boundary, or the boundary can absorb all the energy), an artificial boundary is used according to Reference [2], that is, the boundary conditions are assumed as

$$\sigma = -a\rho C_p \dot{u}_p$$
$$\tau = -b\rho C_s \dot{u}_s$$

In the equations, $\dot{u}_p$ and u_s are velocities of the mass point at normal and tangential directions; C_p and C_s are velocities of the P wave and S wave; and a and b are dimensionless parameters. When a=b=1, the P wave of the arbitrary incident angle absorbs 98.5 percent of the energy; the S wave absorbs 95 percent of the energy. Hence, in addition to the free boundary and load boundary naturally existing, other boundaries in the article use artificial boundaries.

IV. Computation Result

1. General stress trend at circumference of the cave

After one period of oscillation of the mass point, the stress wave propagating in the medium has the superposition phenomenon (refer to the waveform diagram) caused by reflection of the wave. At the side facing detonation in the cave, there is an apparent first stress-peak value; at the back detonation side, there are apparently wave diffraction, interference and structural reaction*. For example, the σ_y value of the juncture point "142" in the wall does not have attenuation in the range of calculation time because of diffraction and interference of the wave.

The stress effect** and reflection phenomenon appear when the stress wave propagates to the vicinity of 1 to 1.5 spans from the cave. However, other points are still similar to those of a free field (Figs. 6 and 8).

---

* This is the reaction of external force, since the cave is considered as a structure.

** This means that due to the existence of the cave, the stress state in the vicinity of the cave is different from that in a free field.

All of the first stress peak values (in the low stress zone of relative safety) in the direction back to the detonation are no greater than the first stress peak values in the direction facing the detonation. Comparing the stress states (Figs. 4, 5 and 10) at both sides of the cave, we can see the apparent asymmetry.

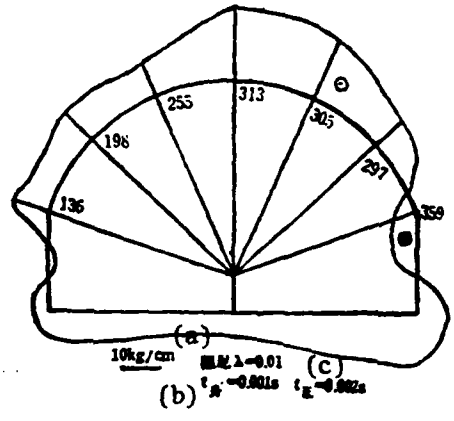

Fig. 4. Radial stress surrounding the cave.
Key: (a) Damping; (b) Ascending; (c) Positive.

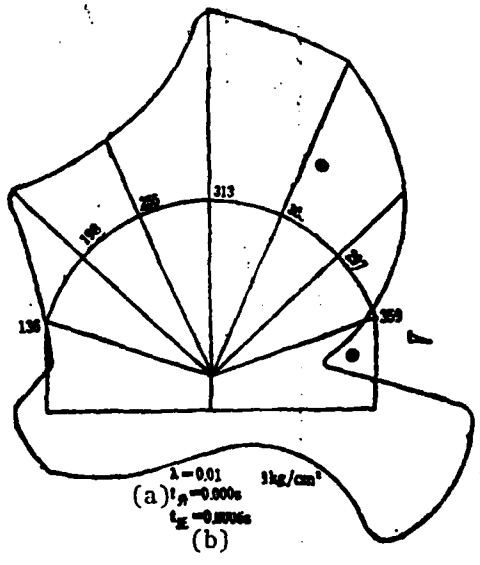

Fig. 5. Radial stress surrounding the cave.
Key: (a) Ascending; (b) Positive.

2. Radial stress at the circumference of the cave

As revealed in Figs. 4 and 5, the stress state has apparent asymmetry at the sides facing and back to the detonation (with the exception of distribution of peak values), but the distribution rules have similarities. At places where abrupt changes of structural shapes occur, at the arch footing and wall corner, abrupt stress changes also occur. In the vicinity of the midpoint of the straight wall, negative signs of stress appear. In most zones at the top of the arch, there is the same stress sign.

The time waveform of stress: at the side facing the detonation, there is an apparent attenuating characteristic of oscillation in stress.

At the direction back to the detonation, this attenuation property still exists but the oscillation property is weakened while the diffraction interference is intensified (refer to the time-waveform diagram).

3. Radial stress of load waveform

Compares Fig. 4 with Fig. 5.

Table 1 shows the case when the stress wavelength is in conformity with the characteristic dimension of the cave, asymmetry appears on the stress reaction of the sides facing and back of the detonation in the cave. When the stress wavelength is further shortened (reducing the time of positive-pressure function of the load waveform), the asymmetry is intensified. As Fig. 4 shows, the value of stress σ_{394y} at the midpoint (juncture point "394") of the straight wall facing the detonation at loading is greater by 17 times than the stress σ_{142y} of the corresponding point (juncture point "142") at the back face of the detonation; the corresponding value for Fig. 5 is 18 times greater in load.

Table 1

(a)荷载波形(毫秒)		(b) 岩洞附近波形 (289结点，距岩洞中心8.5米)		σ_{394y}(公斤/厘米²) (c)	σ_{142y}(公斤/厘米²) (c)	$\sigma_{394y}/\sigma_{142y}$
$t_{升}$(d)	$t_{正}$(e)	$t_{正}$(毫秒)(f)	波 长(米)(g)			
1	2	5.5	13.75	6.054	0.3464	17
0	0.6	3.8	9.50	1.687	0.09434	18

Key: (a) Load waveform (ms); (b) Waveform in the vicinity of cave (at juncture point "289", a distance of 8.5 meters from the center of the cave); (c) kg/cm^2; (d) Ascending; (e) Positive; (f) $t_{positive}$ (ms); (g) Wavelength (m).

For the distribution of stress peak values in the radial direction, the upper portion of the straight wall at the surface facing the detonation is the weak

sector under force (tensile stress), threatened first by the detonation wave; it is possible to be destroyed first.

Although there is stress concentration with corresponding intensity, the sign of peak values is positive pressure, and the location is at the base of the structure. It is estimated that no serious destruction is likely.

4. Stress state above the top of the arch (Figs. 4 and 6)

a. The zone of structure effect is about the range of doubling the span; the other zones have the trend of being in a free field; the stress state is not related to the cave. High stress is only in a very narrow zone the vicinity of the edge of the cave. If the positive stress at the arch to ttenuates rapidly with increasing distance from the surface of the arch (such as the juncture point "313"), the stress one meter deep from the surface reduced from 20.6 kg/cm^2 to 14.4 kg/cm^2, a reduction of 30 percent.

b. The maximum positive stress σ_x exists at the symmetrical surface. The minimum stress also exists at the symmetrical surface.

c. A high stress zone is at the side facing the detonation surface, but the zone is not as apparent as at the side wall.

5. Coefficient of stress concentration

We know by comparing the distribution of stress σ_x at the symmetrical surface of the arch top that the approximation of the stress concentration coefficient at this point is shown in the following equation:

$$\eta = \frac{\sigma_{max}}{\bar{\sigma}_x} \approx 2$$

$\bar{\sigma}_x$ is the value of the free field at the symmetrical surface. Comparing the stress distribution of the lower region of the floor, the coefficient of stress concentration also assumes the aforementioned value.

6. Stress state at side of straight wall facing detonation (Fig. 7)

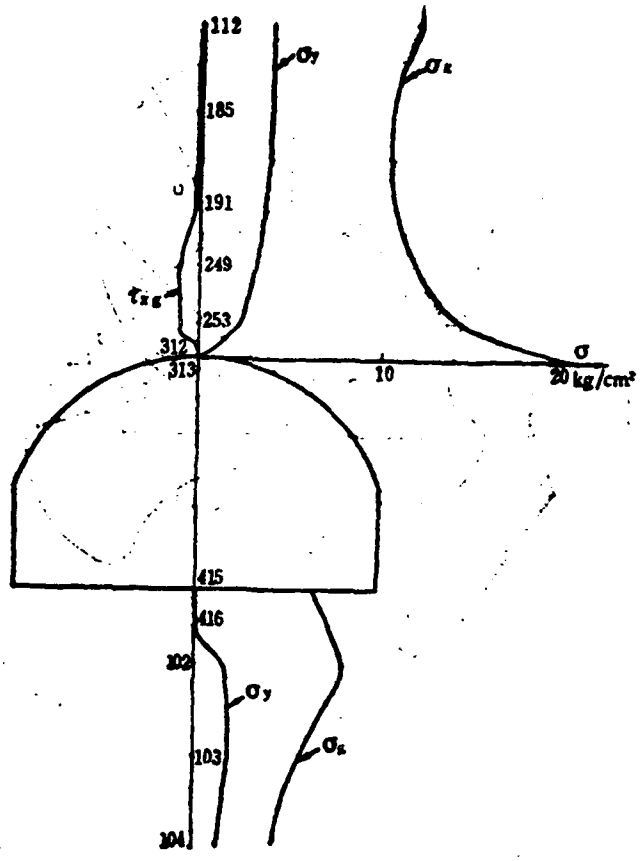

Fig. 6. Stress distribution passing through the 45° axial line at the wall corner along the vertical axial line through the top of the arch.

The cross-section I is 0.46 m from the surface of the cave; cross-section II is 0.92 m from the cave surface; cross-section III is 2.36 m from the cave surface; and cross-section IV is 3.80 m from the cave surface.

a. Positive stress σ_x

Basically, distributions along the y direction at cross-sections III and IV are homogeneous. Along the y direction at cross-sections I and II, the

distribution is also basically homogeneous with the exception of the horizontal zone at the wall corner. The stress concentration of the corner point tends to bend the distribution curve, but the bending apparently weakens with increasing distance.

The variation of σ_x along the x direction is the distribution of a cubic curve in the zone shown in the figure, satisfying the condition that the boundary of the straight wall is zero.

b. Positive stress σ_y

For the variation of σ_y along the x direction, the sign of the stress changes between cross sections I and II; that is, however, not a linear regular variation. Later, the change tends to flatten with increasing x.

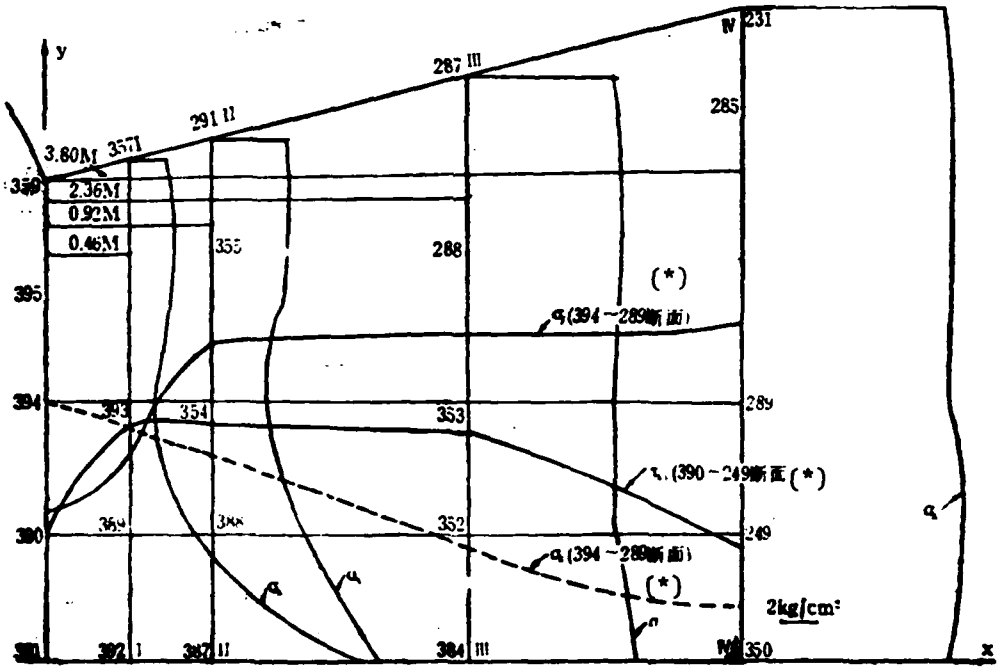

Fig. 7. Stress distribution at the side of the straight wall of the surface facing the detonation.
Key: (*) Cross section.

In the two aforementioned points, the cross-sectional surface of juncture points "394" ∿ "289" (in the x direction) are selected.

c. Shearing stress τ_{xy}

As shown in the figure, there is a parabolic distribution (the distribution curve of cross-sectional surface τ_{xy} of juncture points "390" ∿ "249" in Fig. 7) within the diagram range.

As revealed in the aforementioned, in this zone the stress state has the property of a structural member subject to bending, similar to the beam structure under distribution of the action of a lateral load.

7. Stress of the free field

Along the wave propagation direction, there is very rapid consistent attenuation beginning from the loading point; the stress tends to be more flattened the closer to the cave. In the vicinity of the cave, reflection stress occurs (Fig. 8). If values of these points are shown on double-logarithm coordinates, the trend is closer to linearity between sectors of the free field, but there is deviation in the vicinity of the cave (Fig. 9).

8. Variation of stress-time waveform with distance

For an example of juncture point "367" and juncture point "289" after moving 25 m of time waveform of the juncture point "367", the duration of the positive pressure function of the waveform pulse is increased from 2 ms to 5.5 ms. As pointed out in some papers, the circumference length of the period is a function of dt/T. This is possibly related to the method itself (such as the magnitude of unit selected along the wave propagation direction), and also possibly related to the propagation property of the wave itself. In fact, owing to the influence of various factors, the wave propagation in a rock medium has the phenomenon of a lengthening period (Fig. 10).

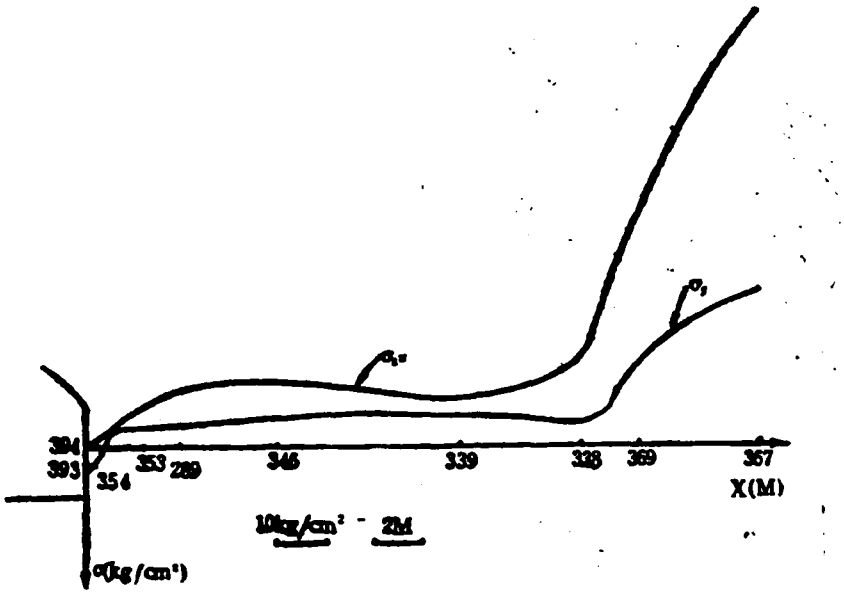

Fig. 8. Attenuation of peak-value stress.

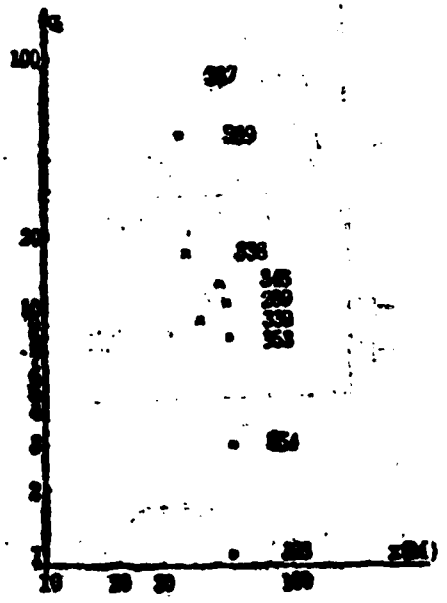

Fig. 9.

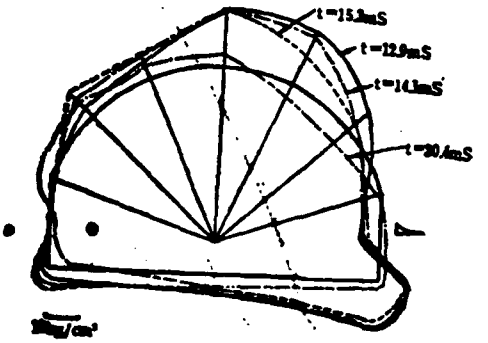

Fig. 10. Variations of radial stress with time.

9. Figure 10 shows the variation states with time of radial stress at the circumference of the cave when the pressure wave passes through the cave. This explains that there is a certain time difference in the value of the stress peak of the surfaces facing and back of the detonation; the variation of stress with time at the top portion of the arch is more intensified.

V. Conclusion

According to the aforementioned discussion, under detonation loading when the wavelength is in conformity with the geometrical property dimensions of the cave, there are the following results:

1. Under detonation loading of an irregular cross-section straight wall of the arch top, the basic rule of the radial stress at the arch top is generally consistent with that of a regular cross section (cylinder).

2. The radial-direction stress peak values appear asymmetric between directions facing and back of the detonation in the cave; the peak values of the facing detonation direction are greater than the direction back to the detonation. The maximum value can be 20 times greater.

3. At the facing detonation surface, the stress-time waveform is more in the form of a simple harmonic curve. Generally, the first peak value is the highest. However, it is relatively complex (with interferences) at the surface back to the detonation. Sometimes, relatively high-value superimposed stress may appear.

4. Under the situation of the computation model in this article, after a period of stress wave propagation, the superimposition phenomenon of the wave occurs.

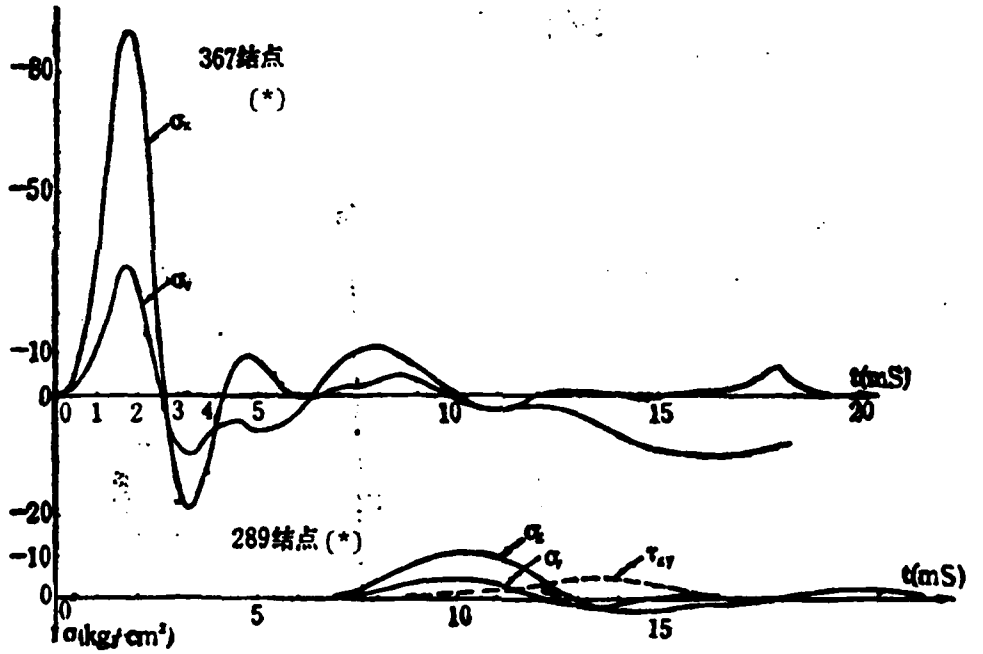

Fig. 11. Diagram of stress waveform.
Key: (*) Juncture point.

5. The structural effect of the cave can only occur when the wave propagates to the vicinity of a double span distance. However, the high (radial) stress zone at the arch top can only occur in the range of less than 1/10 of the span; then the stress rapidly decreases to the state of a free field.

6. The stress state at the (facing detonation) straight wall side is similar to the situation of a structural member (under bending) with bending, extrusion, shearing and other stresses.

7. At the symmetrical surface of the cave, the coefficient of stress concentration is approximately 2.

8. The radial stress has the phenomenon of apparent attenuation with increasing distance. In certain zones (in the free field nearing the loading surface), the attenuation conforms to the index law; in some other zones (in the vicinity of the cave), the attenuation conforms to the cubic curve with the existence of reflection stress.

9. There is relatively greater positive stress and smaller shearing stress in the symmetrical surface of the cave.

10. When the wave passes through the cave, there is a certain time difference in the stress peak values of the facing and back of detonation surface. The stress of the arch top region has more intensified changes with time.

The aforementioned points are obtained from the specified computation conditions of the article; possibly there are limitations and errors.

LITERATURE

[1]Stability and Accuracy Analysis of Direct Integration Methods, K. J. Bathe, E. L. Wilson'Eathquake Enginerring and Structural Dynamics' Vol.1.№3 283~291 (1973)
[2]Finite dynamic model for infinite media by John Lysmer, M. ASCE and Roger L. Kuhlemeyer, A. M. ASCE, Engineering Mechanics Division, Vol. 95 No EM4. 857~877 (1969)

DISTRIBUTION LIST

DISTRIBUTION DIRECT TO RECIPIENT

ORGANIZATION	MICROFICHE
A205 DMAHTC	1
A210 DMAAC	1
B344 DIA/RTS-2C	9
C043 USAMIIA	1
C500 TRADOC	1
C509 BALLISTIC RES LAB	1
C510 R&T LABS/AVRADCOM	1
C513 ARRADCOM	1
C535 AVRADCOM/TSARCOM	1
C539 TRASANA	1
C591 FSTC	4
C619 MIA REDSTONE	1
D008 NISC	1
E053 HQ USAF/INET	1
E403 AFSC/INA	1
E404 AEDC/DOF	1
E408 AFWL	1
E410 AD/IND	1
E429 SD/IND	1
P005 DOE/ISA/DDI	1
P050 CIA/OCR/ADD/SD	2
AFIT/LDE	1
FTD	
CCN	1
NIA/PHS	1
NIIS	2
LLNL/Code L-389	1
NASA/NST-44	1
NSA/1213/TDL	2

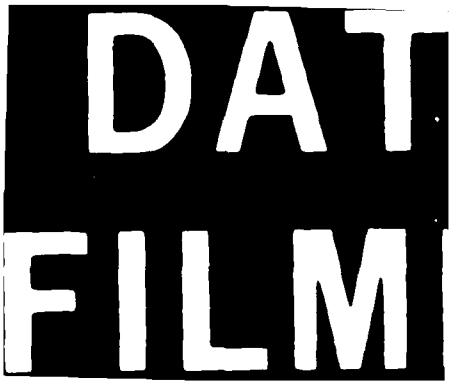
DAT
FILM